



HAL
open science

Time-resolved detection of single-electron interference

S. Gustavsson, R. Leturcq, M. Studer, T. Ihn, K. Ensslin, D.C. Driscoll, A.C. Gossard

► **To cite this version:**

S. Gustavsson, R. Leturcq, M. Studer, T. Ihn, K. Ensslin, et al.. Time-resolved detection of single-electron interference. *Nano Letters*, 2008, 8, pp.2547-2550. 10.1021/nl801689t . hal-00357780

HAL Id: hal-00357780

<https://hal.science/hal-00357780>

Submitted on 15 Jul 2022

HAL is a multi-disciplinary open access archive for the deposit and dissemination of scientific research documents, whether they are published or not. The documents may come from teaching and research institutions in France or abroad, or from public or private research centers.

L'archive ouverte pluridisciplinaire **HAL**, est destinée au dépôt et à la diffusion de documents scientifiques de niveau recherche, publiés ou non, émanant des établissements d'enseignement et de recherche français ou étrangers, des laboratoires publics ou privés.

Time-resolved detection of single-electron interference

S. Gustavsson,* R. Leturcq, M. Studer, T. Ihn, and K. Ensslin
Solid State Physics Laboratory, ETH Zürich, CH-8093 Zürich, Switzerland

D. C. Driscoll and A. C. Gossard
Materials Department, University of California, Santa Barbara, CA-93106, USA
(Dated: October 30, 2018)

We demonstrate real-time detection of self-interfering electrons in a double quantum dot embedded in an Aharonov-Bohm interferometer, with visibility approaching unity. We use a quantum point contact as a charge detector to perform time-resolved measurements of single-electron tunneling. With increased bias voltage, the quantum point contact exerts a back-action on the interferometer leading to decoherence. We attribute this to emission of radiation from the quantum point contact, which drives non-coherent electronic transitions in the quantum dots.

One of the cornerstone concepts of quantum mechanics is the superposition principle as demonstrated in the double-slit experiment [1]. The partial waves of individual particles passing a double slit interfere with each other. The ensemble average of many particles detected on a screen agrees with the interference pattern calculated using propagating waves [Fig. 1(a)]. This has been demonstrated for photons, electrons in vacuum [2, 3] as well as for more massive objects like C_{60} -molecules [4]. The Aharonov-Bohm (AB) geometry provides an analogous experiment in solid-state systems [5]. Partial waves passing the arms of a ring acquire a phase difference due to a magnetic flux, enclosed by the two paths [Fig. 1(b)]. Here we demonstrate the self-interference of individual electrons in a sub-micron Aharonov-Bohm interferometer. The interference pattern is obtained by counting individual electrons passing through the structure.

We first discuss the experimental conditions necessary for observing single-electron AB interference. We make use of a geometry containing two quantum dots (QD) within the AB-ring. Figure 1(c) shows the structure with two QDs (marked by 1 and 2) tunnel-coupled via two separate barriers. The sample was fabricated by local oxidation [6] of the surface of a GaAs/AlGaAs heterostructure containing a two-dimensional electron gas 34 nm below the surface. More details about the structure are given in Ref. [7]. Following the sketch in Fig. 1(b), electrons are provided from the source lead, tunnel into QD1 and pass on to QD2 through either of the two arms. Upon arriving in QD2, the electrons are detected in real-time by operating a near-by quantum point contact (QPC) as a charge detector [8]. Coulomb blockade prohibits more than one excess electron to populate the structure, implying that the first electron must leave to the drain before a new one can enter. This enables time-resolved operation of the charge detector and ensures that we measure interference due to individual electrons.

To avoid dephasing, the electrons should spend a time as short as possible on their way from source to QD2.

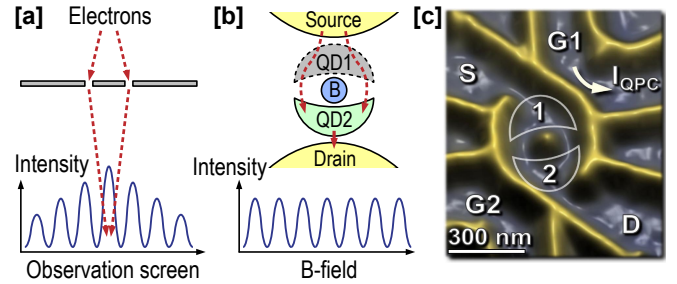


FIG. 1: (a) Setup of a traditional double-slit experiment. Electrons passing through the two slits give rise to interference pattern on the observation screen. (b) Schematic drawing of the setup used for measuring single-electron Aharonov-Bohm interference. Electrons are injected from the source lead, tunnel through QD1 and end up in QD2, where they are detected. The interference pattern is due to the applied B-field, which introduces a phase difference between the left and right arm connecting the two quantum dots. (c) Double quantum dot used in the experiment. Yellow lines are written with a scanning force microscope on top of a semiconductor heterostructure and represent the potential landscape for the electrons. The QDs (marked by 1 and 2) are connected by two separate arms, allowing partial waves taking different paths to interfere. The current in the nearby QPC (I_{QPC}) is used to monitor the electron population in the system.

This is achieved by raising the electrochemical potential of QD1 so that electrons in the source lead lack an energy δ required for entering QD1 [see Fig. 2(c)]. The time-energy uncertainty principle still allows electrons to tunnel from source to QD2 by means of a second order process. The electron dwell time in QD1 is then limited to a short time scale set by the uncertainty relation, with $t = \hbar/\delta$ [9].

The charge detector is implemented by tuning the QPC conductance close to $0.5 \times 2e^2/h$. At this point the QPC conductance is highly sensitive to changes in its electrostatic surroundings, allowing it to be used to detect single electrons tunneling into or out of the QD in real time [10, 11, 12]. The QPC conductance was measured by applying a d.c. bias voltage over the QPC, $V_{QPC} = 250 \mu\text{V}$, and monitoring the current I_{QPC} . The charge detection

*Electronic address: simongus@phys.ethz.ch

technique allows the tunneling rates for electrons entering and leaving the double QD (DQD) to be determined separately [13, 14].

In the experiment, we apply appropriate gate voltages to tune the tunneling rates between the DQD and the source and drain leads to values below 15 kHz. The tunnel couplings between the QDs are set to a few GHz. The interdot transitions are too fast to be detected with the bandwidth of the charge detector ($\Gamma_{\text{det.}} = 20$ kHz), but the coupling energy can still be determined from charge localization measurements [15].

Figure 2(a) shows the charge stability diagram of the DQD, measured by counting electrons entering and leaving the structure within a fixed period of time. The data was taken with $600 \mu\text{V}$ bias applied between source and drain. The hexagon pattern together with the triangles of electron transport appearing due to the applied bias are well-known characteristics of DQD systems [16]. Between the triangles, there are band-shaped regions with weak but non-zero count rates where electron tunneling is expected to be suppressed due to Coulomb blockade. The finite count rate in these regions can be attributed to electron tunneling involving virtual processes [17].

To investigate these processes in more detail, we follow the lines of Ref. [17] and plot the rates for electrons tunneling into and out of the DQD measured along the dashed line in Fig. 2(a). The result is shown in Fig. 2(b). Going along the dashed line in Fig. 2(a) corresponds to lowering the electrochemical potential of QD1 while keeping the potential of QD2 constant. In the region marked by I, electrons tunnel sequentially from the source into QD1, continue from QD1 to QD2 and finally leave QD2 to the drain lead. Proceeding to point II in Fig. 2(a, b), the electrochemical potential of QD1 is lowered and an electron is trapped in QD1 [see sketch in Fig. 2(c)]. The electron lacks an energy δ_a to leave to QD2, but because of time-energy uncertainty there is a time-window of length $\sim \hbar/\delta_a$ within which tunneling from QD1 to QD2 followed by tunneling from the source into QD1 is possible without violating energy conservation. An analogous process is possible involving the next unoccupied state of QD1, occurring on timescales $\sim \hbar/\delta_b$. The processes correspond to electron *cotunneling* from the source lead to QD2. By continuing to point III, the unoccupied state of QD1 is shifted into the bias window and electron transport is again sequential.

The solid lines in Fig. 2(b) show the tunneling rates expected from sequential tunneling [18]. The fit gives the tunnel couplings between source and the occupied (Γ_{Sa})/unoccupied (Γ_{Sb}) states of QD1, with $\Gamma_{\text{Sa}} = 6.4$ kHz and $\Gamma_{\text{Sb}} = 14$ kHz. In the cotunneling regions we fit the data to an expression involving the sum of the two cotunneling processes [9, 17]:

$$\Gamma_{\text{cot}} = \Gamma_{\text{Sa}} t_a^2 / \delta_a^2 + \Gamma_{\text{Sb}} t_b^2 / \delta_b^2. \quad (1)$$

Here, t_a , t_b are the tunnel couplings between the occupied/unoccupied states in QD1 and the state in QD2. The values for Γ_{Sa} and Γ_{Sb} are taken from measure-

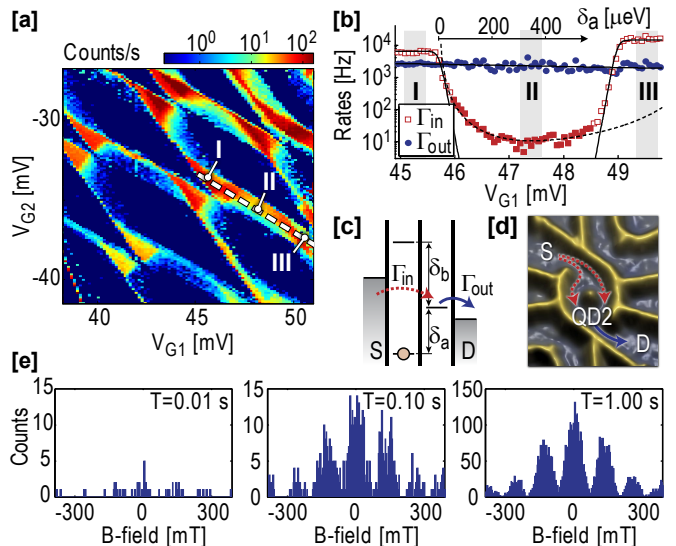


FIG. 2: (a) Charge stability diagram of the double quantum dot, recorded by counting electrons entering and leaving the structure. The data was taken at bias voltage $V_b = 600 \mu\text{V}$ and $B = 0$ T. (b) Tunneling rates for electrons entering (red) and leaving (blue) the DQD, measured along the dashed white line in (a). The upper x-axis shows δ_a , the potential difference between the state in QD2 and the occupied state of QD1. The solid lines are tunneling rates expected from sequential tunneling, while the dashed line is a fit to the cotunneling model of Eq. (1). Parameters are given in the text. The data was taken with $B = 340$ mT. (c) Energy level configuration of the DQD at the point marked by II in (a, b). Electron transport from source to QD2 is possible by means of cotunneling. (d) Schematic drawing of the cotunneling process. (e) Number of electrons arriving at QD2 within the fixed period of time indicated in the upper-right corner, measured as a function of magnetic field. The data was taken at point II in (a). The count rate shows an oscillatory pattern with a visibility higher than 90%.

ment in the sequential regimes. The dashed line in Fig. 2(b) shows the results of Eq. (1), with fitting parameters $t_a = 8.3 \mu\text{eV}$ and $t_b = 13 \mu\text{eV}$. These values are in good agreement with values obtained from the charge localization measurements. We emphasize that Eq. (1) is valid only if $\delta_a, \delta_b \gg t_a, t_b$ and if sequential transport is sufficiently suppressed, i.e. in the range $46 \text{ mV} < V_{G1} < 48.6 \text{ mV}$ of Fig. 2(b).

Coming back to the sketch of Fig. 1(b), we note that the cotunneling configuration of case II in Fig. 2(a-c) is ideal for investigating the Aharonov-Bohm effect for single electrons. Due to the low probability of the cotunneling process, the source lead provides low-frequency injection of single electrons into the DQD. The injected electrons cotunnel through QD1 into QD2 on a timescale $t \sim \hbar/\delta \sim 1$ ps much shorter than typical decoherence times of the system [19]. This ensures that phase coherence is preserved. Finally, the electron stays in QD2 for a time long enough to be registered by the finite-bandwidth charge detector. The tunneling processes are visualized

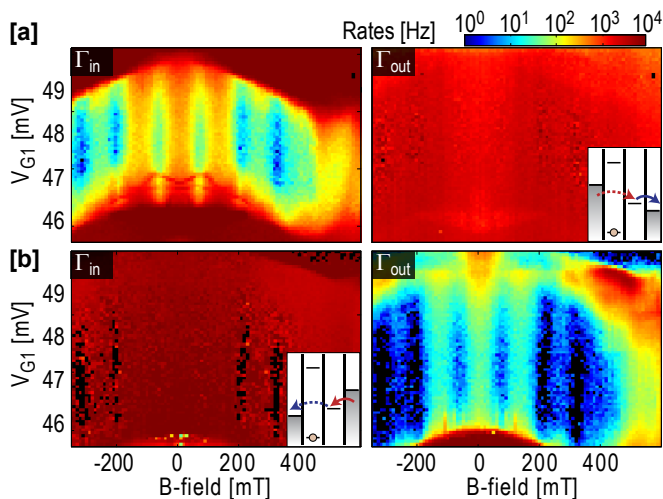


FIG. 3: (a) Tunneling rates for electrons entering (Γ_{in}) and leaving (Γ_{out}) the DQD, measured versus electrochemical potential of QD1 and magnetic field. The y-axis corresponds to sweeps along the dashed line in Fig. 2(a). Within the cotunneling region, Γ_{in} shows clear B-field periodicity, while Γ_{out} remains constant. This is in agreement with the picture where only the electrons tunneling from source to QD2 encircle the Aharonov-Bohm ring, while electrons leaving to drain remains unaffected by the applied B-field. (b) Same as (a), but with reverse bias over the DQD. Here, the roles of Γ_{in} and Γ_{out} are inverted.

in Fig. 2(d).

To proceed, we tune the system to case II of Fig. 2(a, b) and count electrons as a function of magnetic field. Figure 2(e) shows snapshots of the number of electrons arriving in QD2 after three different times. The electrons travel one-by-one through the system but still build up a well-pronounced interference pattern with period 130 mT. This corresponds well to one flux quantum $\Phi = h/e$ penetrating the area enclosed by the two paths. The visibility of the AB-oscillations is higher than 90%, which is a remarkably large number demonstrating the high degree of phase coherence in the system. We attribute the high visibility to the short time available for the cotunneling process [20] and to strong suppression of electrons being backscattered in the reverse direction, which is otherwise present in AB-experiments. Another requirement for the high visibility is that the two tunnel barriers connecting the QDs are carefully symmetrized. The overall decay of the maxima of the AB-oscillation with increasing B is probably due to magnetic field effects on the orbital wavefunctions in QD1 and QD2.

Figure 3(a) shows the separate rates for electrons tunneling into and out of the DQD as a function of magnetic field. The y-axis corresponds to the dashed line in Fig. 2(a), i.e., to the energy of the states in QD1. The measurement shows a general shift of the DQD energy with the applied B-field, which we attribute to changes of the orbital wavefunctions in the individual QDs. Within the cotunneling region, Γ_{in} shows well-defined B-periodic

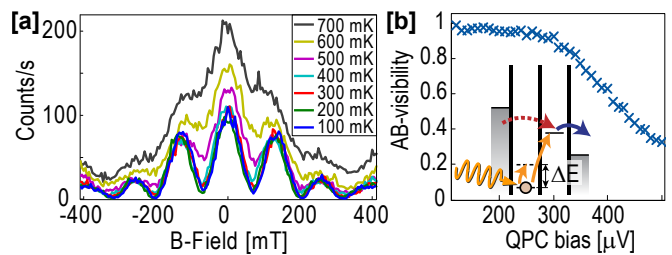


FIG. 4: (a) Aharonov-Bohm (AB) oscillations measured at different temperatures. At ~ 400 mK, the visibility of the oscillations drops drastically. The data was taken along the dashed line in (b). (b) Amplitude of AB-oscillations measured at different QPC bias. The inset shows a few photon absorption processes that are possible at large QPC bias.

oscillations. At the same time, Γ_{out} is essentially independent of the applied field. This is expected since Γ_{out} measures the rate at which electrons leave QD2 to the drain, which occurs independently of the magnetic flux passing through the AB-ring [see Fig. 2(c, d)]. In Fig. 3(b), the bias over the DQD is reversed. This inverts the roles of Γ_{in} and Γ_{out} so that Γ_{out} corresponds to the cotunneling process. Consequently Γ_{out} shows B-periodic oscillations while Γ_{in} remains unaffected. In the black regions seen in Fig. 3(b) no counts were registered within the measurement time of three seconds due to strong destructive interference for the tunneling-out process. As a consequence we could not determine the tunneling rates in those regions.

In Fig. 4(a), we investigate how the AB-oscillations are influenced by elevated temperatures. The dephasing of open QD systems is thought to be due to electron-electron interaction [21], giving dephasing rates that depend strongly on temperature [22]. Figure 3(a) shows the temperature dependence of the AB oscillations in our system. The amplitude of the oscillations remains almost unaffected up to ~ 400 mK, indicating that the coherence is not affected by temperature until the thermal energy becomes comparable to the single-level spacing of the QDs. We conclude that the decreased visibility at higher temperatures is due to an increase in thermal fluctuations of the QD population.

Decoherence can also occur because of interactions with the environment. In the experiment, we use the current in the QPC to detect the charge distribution in the DQD. In principle, the QPC could also determine whether an electron passed through the left or the right arm of the ring, thus acting as a which-path detector [23, 24]. If the QPC were to detect the electron passing in one of the arms, the interference pattern should disappear. In Fig. 4(b), we show the visibility of the AB-oscillations as a function of bias on the QPC. The visibility remains unaffected up to $V_{\text{QPC}} \sim 250 \mu\text{eV}$, but drops for higher bias voltages.

We argue that the reduced visibility is not due to which-path detection. At $V_{\text{QPC}} = 400 \mu\text{V}$, the current through the QPC is approximately 10 nA. This gives

an average time delay between two electrons passing the QPC of $e/I_{\text{QPC}} \sim 16$ ps. Since this is ten times larger than the typical cotunneling time, it is unlikely that the electrons in the QPC are capable of performing an effective which-path measurement. Instead, we attribute the decrease of the AB-visibility to processes where the DQD absorbs photons emitted from the QPC. Previous work has shown that such processes may indeed excite an electron from one QD to the other, as long as the energy difference between the QDs is lower than the energy provided by the QPC bias [7]. The radiation of the QPC may also drive transitions within the individual QDs, thus putting one of the QDs into an excited state [25, 26]. A few absorption processes are sketched in the inset of Fig. 4(b).

As long as the QPC bias is lower than both the DQD detuning ($\delta = 400 \mu\text{eV}$) and the single-level spacing of the individual QDs ($\Delta E \sim 200 \mu\text{eV}$), the AB visibility in Fig. 4(b) is close to unity. When raising the QPC bias above ΔE , we start exciting the individual QDs. With increased QPC bias, more states become available and the absorption process becomes more efficient. This

introduces new virtual paths for the cotunneling process. Since the different paths may interfere destructively, the interference pattern is eventually washed out. In this way, the QPC has a physical back-action on the measurement which is different from informational back-action [27] and which-path detection previously investigated [23, 24].

In summary, we have demonstrated interference of single electrons in a solid state environment. Such experiments have so far been limited to photons or massive particles in a high-vacuum environment in order to decouple the quantum mechanical degrees of freedom as much as possible from the environment. Our experiments demonstrate the exquisite control of modern semiconductor nanostructures which enables interference experiment at the level of single quasi-particles in a solid state environment. Once extended to include spin degrees of freedom [28] such experiments have the potential to facilitate entanglement detection [29] or investigate the interference of particles [30] originating from different sources.

-
- [1] T. Young, Philosophical Transactions of the Royal Society of London **94**, 1 (1804).
- [2] C. Jönsson, Z. Physik **161**, 454 (1961).
- [3] A. Tonomura, J. Endo, T. Matsuda, T. Kawasaki, and H. Ezawa, Am. J. Phys. **57**, 117 (1989).
- [4] M. Arndt, O. Nairz, J. Vos-Andreae, C. Keller, G. van der Zouw, and A. Zeilinger, Nature **401**, 680 (1999).
- [5] Y. Aharonov and D. Bohm, Phys. Rev. **115**, 485 (1959).
- [6] A. Fuhrer, A. Dorn, S. Lüscher, T. Heinzel, K. Ensslin, W. Wegscheider, and M. Bichler, Superl. and Microstruc. **31**, 19 (2002).
- [7] S. Gustavsson, M. Studer, R. Leturcq, T. Ihn, K. Ensslin, D. C. Driscoll, and A. C. Gossard, Phys. Rev. Lett. **99**, 206804 (2007).
- [8] M. Field, C. G. Smith, M. Pepper, D. A. Ritchie, J. E. F. Frost, G. A. C. Jones, and D. G. Hasko, Phys. Rev. Lett. **70**, 1311 (1993).
- [9] D. V. Averin and Y. V. Nazarov, *Single Charge Tunneling* (Plenum, New York, 1992).
- [10] L. M. K. Vandersypen, J. M. Elzerman, R. N. Schouten, L. H. Willems van Beveren, R. Hanson, and L. P. Kouwenhoven, Appl. Phys. Lett. **85**, 4394 (2004).
- [11] R. Schleser, E. Ruh, T. Ihn, K. Ensslin, D. C. Driscoll, and A. C. Gossard, Appl. Phys. Lett. **85**, 2005 (2004).
- [12] T. Fujisawa, T. Hayashi, Y. Hirayama, H. D. Cheong, and Y. H. Jeong, Appl. Phys. Lett. **84**, 2343 (2004).
- [13] S. Gustavsson, R. Leturcq, B. Simovic, R. Schleser, T. Ihn, P. Studerus, K. Ensslin, D. C. Driscoll, and A. C. Gossard, Phys. Rev. Lett. **96**, 076605 (2006).
- [14] O. Naaman and J. Aumentado, Phys. Rev. Lett. **96**, 100201 (2006).
- [15] L. DiCarlo, H. J. Lynch, A. C. Johnson, L. I. Childress, K. Crockett, C. M. Marcus, M. P. Hanson, and A. C. Gossard, Phys. Rev. Lett. **92**, 226801 (2004).
- [16] W. G. van der Wiel, S. De Franceschi, J. M. Elzerman, T. Fujisawa, S. Tarucha, and L. P. Kouwenhoven, Rev. Mod. Phys. **75**, 1 (2002).
- [17] S. Gustavsson, M. Studer, R. Leturcq, T. Ihn, K. Ensslin, D. C. Driscoll, and A. C. Gossard (2008), arXiv.org:0805.3395.
- [18] L. P. Kouwenhoven, C. M. Marcus, P. M. McEuen, S. Tarucha, R. M. Westervelt, and N. S. Wingreen, in *Mesoscopic Electron Transport*, edited by L. L. Sohn, L. P. Kouwenhoven, and G. Schön (Kluwer, Dordrecht, 1997), NATO ASI Ser. E 345, pp. 105–214.
- [19] E. Eisenberg, K. Held, and B. L. Altshuler, Phys. Rev. Lett. **88**, 136801 (2002).
- [20] M. Sigrist, T. Ihn, K. Ensslin, D. Loss, M. Reinwald, and W. Wegscheider, Phys. Rev. Lett. **96**, 036804 (2006).
- [21] B. L. Altshuler, Y. Gefen, A. Kamenev, and L. S. Levitov, Phys. Rev. Lett. **78**, 2803 (1997).
- [22] A. G. Huibers, M. Switkes, C. M. Marcus, K. Campman, and A. C. Gossard, Phys. Rev. Lett. **81**, 200 (1998).
- [23] E. Buks, R. Schuster, M. Heiblum, D. Mahalu, and V. Umansky, Nature **391**, 871 (1998).
- [24] I. Neder, M. Heiblum, D. Mahalu, and V. Umansky, Phys. Rev. Lett. **98**, 036803 (2007).
- [25] E. Onac, F. Balestro, L. H. W. van Beveren, U. Hartmann, Y. V. Nazarov, and L. P. Kouwenhoven, Phys. Rev. Lett. **96**, 176601 (2006).
- [26] S. Gustavsson, I. Shorubalko, R. Leturcq, T. Ihn, K. Ensslin, and S. Schon (2008), arXiv.org:0805.1341.
- [27] E. V. Sukhorukov, A. N. Jordan, S. Gustavsson, R. Leturcq, T. Ihn, and K. Ensslin, Nature Physics **3**, 243 (2007).
- [28] D. Loss and E. V. Sukhorukov, Phys. Rev. Lett. **84**, 1035 (2000).
- [29] D. S. Saraga and D. Loss, Phys. Rev. Lett. **90**, 166803 (2003).
- [30] I. Neder, N. Ofek, Y. Chung, M. Heiblum, D. Mahalu,

and V. Umansky, *Nature* **448**, 333 (2007).